Accurate Sizing of Nanoparticles Using Confocal Correlation Spectroscopy

Christopher L. Kuyper, Bryant S. Fujimoto, Yiqiong Zhao, Perry G. Schiro, and Daniel T. Chiu*

Department of Chemistry, University of Washington, Seattle, Washington 98195-1700

Received: July 29, 2006; In Final Form: September 21, 2006

The ability to accurately size low concentrations of nanoscale particles in small volumes is useful for a broad range of disciplines. Here, we characterize confocal correlation spectroscopy (CCS), which is capable of measuring the sizes of both fluorescent and nonfluorescent particles, such as quantum dots, gold colloids, latex spheres, and fluorescent beads. We accurately measured particles ranging in diameter from 11 to 300 nm, a size range that had been difficult to probe, owing to a phenomenon coined biased diffusion that causes diffusion times, or particle size, to deviate as a function of laser power. At low powers, artifacts mimicking biased diffusion are caused by saturation of the detector, which is especially problematic when probing highly fluorescent or highly scattering nanoparticles. However, at higher powers (>1 mW), autocorrelation curves in both resonant and nonresonant conditions show a structure indicative of an increased contribution from longer correlation times coupled with a decrease in shorter correlation times. We propose that this change in the autocorrelation curve is due to the partial trapping of the particles as they transit the probe volume. Furthermore, we found only a slight difference in the effect of biased diffusion when comparing resonant and nonresonant conditions. Simulations suggest the depth of trapping potential necessary for biased diffusion is >1k_BT. Overcoming artifacts from detector saturation and biased diffusion, CCS is particularly advantageous due to its ability to size particles in the small volumes characteristic of microfluidic channels and aqueous microdroplets. We believe the method will find increasing use in a wide range of applications in measuring nanoparticles and macromolecular systems.

Introduction

The accurate characterization of nanoscale particles has wide application in several cross-disciplinary fields. For example, liposomes and other nanocontainers are used effectively as agents for isolation and controlled delivery of drugs and genes to treat specific regions of the body.[1,2] In addition, nanoscale investigation of subcellular structures offers new insights into roles that size or shape may play in cellular processes, such as the release of synaptic-vesicle contents at synapses.[3] Furthermore, synthetic nanoparticles composed of materials such as polymers or metals are finding broad utility in a range of applications such as diagnostic imaging.[4,5] In many cases, the unique chemical and physical properties of nanoparticles results from not only their material characteristics but also their size and shape. Currently, detailed imaging of nanoscale particles is performed using microscopy techniques such as scanning electron microscopy (SEM), atomic force microscopy (AFM), transmission electron microscopy (TEM), and cryogenic electron microscopy (cryo-EM), which achieve atomic to micrometer scale resolution for the visualization of particle morphologies.[6,7] Unfortunately, these approaches are not ideal in some cases because long preparation times are needed to acquire images, the use of expensive equipment is required, and for SEM/TEM, samples must be dried in ultrahigh vacuum and particles must be conductive or coated in gold to image at nanometer resolutions. Furthermore, fixing samples for imaging with cryo-EM or adsorbing the particles on a surface for AFM can result

in morphological deformation, thus giving rise to inaccurate or misleading measurements.

For many applications, direct measurement of freely diffusing particles in solution is more convenient, provides a noninvasive way to gather data in real-time, and offers a means to size samples not suited for imaging with static methods. Dynamic light scattering, perhaps the most popular method for sizing nanoparticles, has been successful owing to its ability to accurately size particles ranging from nanometers to micrometers and because it utilizes relatively inexpensive equipment and hasapplicability to many different types of samples such as synthetic nanoparticles, DNA, and liposomes.[8] In addition to size, analysis at multiple scattering angles can also reveal shape information. Unfortunately, dynamic light scattering is limited to higher concentrations (μM) and requires rather large sample volumes (mL) to avoid artifacts caused by scattering offsurrounding surfaces near the probe volume. These disadvantages are particularly important when considering the increasing number of applications involving nanoparticle synthesis in microfluidic channels,[9−13] encapsulation of particles in immiscible fluid droplets,[14,15] and biological samples that after purification are too dilute and must be analyzed in small-volume aliquots.

As a complementary approach to dynamic light scattering, fluorescence correlation spectroscopy (FCS) can be used to determine rates of movement for very small species at the molecular or large-protein size scale.[16−19] Owing to impressive signal-to-noise ratios characteristic of confocal systems, the method is particularly suited for measuring single fluorescent molecules at low concentrations (pM−nM), and because the probe volume is typically on the order of 0.3 fL very little

* To whom correspondence should be addressed. E-mail: chiu@chem.washington.edu.

sample volume is needed for analysis. In the analysis of larger particles ranging in diameter from tens to hundreds of nanometers, obtaining accurate diffusion coefficients or sizes can be problematic because diffusion times appear to be power dependent. This phenomenon has been coined biased diffusion and is believed to originate from optical trapping forces imparted onto particles as they enter into the laser beam thus slowing the trajectory of the particle in the beam vicinity.[20-23] Not only does the effect appear to slow diffusion, but the probability of the particle entering the probe volume, which is governed by Poisson statistics, also deviates as laser power is increased, causing particles to look as if they are locally concentrated near the laser beam waist.

Here, we characterize confocal correlation spectroscopy (CCS), a method built on the foundation of FCS and capable of accurately sizing particles that are either fluorescent or nonfluorescent.[24] We provide insights into the effects of true and apparent biased diffusion over a wide range of laser powers and present new findings as to how to overcome such artifacts. We found that for bright particles with peak photon count rates in the megahertz range under low excitation powers (nanowatts to microwatts), size dependence on power was due only to detector saturation. The dead time of the detection system has long been known to be a potential source of problems for photon counting experiments including FCS experiments.[17,25,26] Expressions for the effect of the detector dead time on the FCS correlation function have been derived to first order in the ratio of the detector dead time to the sample interval.[17,26] However, the count rates for some of our laser powers were so large that it was not clear if these expressions would still be valid, so the effect of the detector dead time was studied by Monte Carlo simulations, which fit well to the data.

At powers >1 mW, we observed, under resonant and nonresonant conditions, correlation curves with an increase in longer duration bursts or particle transit times coupled with a corresponding decrease in shorter bursts, thus suggesting the occurrence of biased diffusion. Moreover, simulations suggest that biased diffusion did not occur until potential well depths of >$1k_BT$ were reached. Awareness of the power ranges that result in biased diffusion should provide a convenient means to recognize particle interactions with the laser beam. Compared with other sizing techniques, such as dynamic light scattering, the advantage of CCS lies in its ability to measure dilute samples (down to a single particle or molecule) in small volumes (femtoliters). With advances in nonfluorescent modes of single-particle and single-molecule detection, we believe correlation spectroscopy will find increasingly broad use in measuring the dimensions of nanoparticles and macromolecular systems.

Experimental Methods

Materials. Fluorescent (60, 110, 180, and 290 nm) and nonfluorescent (110, 180, and 300 nm) polystyrene beads were purchased from Molecular Probes (Eugene, OR), Duke Scientific Corporation (Palo Alto, CA), and Bangs Laboratories (Fishers, IN). Gold nanoparticles (40, 60, and 110 nm) were from Ted Pella, Inc. (Redding, CA). Quantum dots (QDs), which emitted at 565 nm and were composed of a CdSe core capped with carboxyl-terminated polymer, were purchased from Invitrogen Corporation (Carlsbad, CA).

Experimental Setup. Experiments were conducted on a Nikon TE2000U microscope equipped with a home-built add-on for confocal microscopy. For excitation, 488 nm light from a solid-state diode pumped laser (Coherent Sapphire, Santa Clara, CA) was collimated and directed into a Nikon 100×

objective (NA 1.45). Laser power was measured immediately prior to the beam entering the objective. Fluorescence from the object plane was collected with the objective, passed through a dichroic mirror (z488rdc, Chroma, Rockingham, VT), imaged onto a 50 μm pinhole (Thorlabs, Inc., Newton, NJ), placed at the image plane, and filtered with a band-pass filter (HQ550/100M, Chroma, Rockingham, VT) before being focused onto the avalanche photodiode (APD) (SPCM-AQR-16, Perkin-Elmer, Fremont, CA). Scattering bursts were collected through the same beam path but without a band-pass filter. For nonresonant conditions, we used a 632.8 nm HeNe laser (Coherent, Santa Clara, CA), which was overlaid with the beam focus of the 488 nm laser. Autocorrelation was recorded using a Flex02-12D multiple-tau autocorrelator from correlator.com (Bridgewater, NJ) and fitted with data analysis software. A power meter (PD 300-UV, Ophir Optronics, Wilmington, MA) was used to record laser power before entrance into the objective.

Theory of Confocal Correlation Spectroscopy. Most commonly, confocal correlation spectroscopy has been performed in the fluorescence mode to determine diffusion coefficients of fluorescent particles and molecules undergoing Brownian motion. Here, accurate information was also recorded in a confocal geometry from backscattered bursts off nonfluorescent nanoparticles. Photon bursts corresponding to particles passing through the laser probe volume were autocorrelated, and the resulting correlation curve was fit with the following equation[16]

$$G(\tau) = G_0\left(1 + \frac{\tau}{\tau_D}\right)^{-1}\left(1 + \frac{\tau}{K^2\tau_D}\right)^{-(1/2)} + G_\infty \qquad \tau_D = \frac{w_0^2}{4D} \tag{1}$$

where G_0 is the amplitude of the correlation function, which for an ideal system is inversely proportional to the average number of particles in the probe volume, G_∞ equals 1 for an ideal system, K is the shape factor or the ratio of height (z_0) to width (w_0) of the probe volume, and D is the diffusion coefficient for the fluorescent or nonfluorescent species. Dimensions of the probe volume were determined by calibration with particles of three known sizes (diameters of 110, 180, and 300 nm). Dimensions for the backscattering mode (w_0, 230 nm; z_0, 1 μm) were smaller than those for fluorescence measurements (w_0, 280 nm; z_0, 1.25 μm), which may have been due to a directional dependence of scattering. The measured diffusion time, τ_D, was used to calculate the diffusion coefficient (D) and the particles' radius (R) using the Stokes–Einstein equation ($D = k_BT/6\pi\eta R$), where k_B is the Boltzmann constant, T is temperature, and η is viscosity of the surrounding medium.

Simulations of Effects of Detector Dead Time. Simulations similar to those used previously were performed to test the effect of the detector dead time.[19] The sample was modeled as fluorescent beads with a radius of 55 nm in a container, which was a sphere of radius $R = 3\,000$ nm. There were 40 beads in the container, which corresponded to a concentration of 0.6 nM. The simulation temperature was 20 °C. A trial configuration was created for each time step in the simulation by applying a small random displacement to each of the particles. Three random deviates, uniformly distributed between $-\epsilon_0$ and $+\epsilon_0$, were chosen for each particle to give random displacements of the particle along the $x, y,$ and z directions. The random number generator RANLUX was used to generate the random deviates.[27] The relationship between the time step size, Δt, and the translation diffusion coefficient, D, is the following[28]

Accurate Sizing of Nanoparticles

J. Phys. Chem. B, Vol. 110, No. 48, 2006 **24435**

$$\Delta t = \frac{\langle \epsilon^2 \rangle}{2D} \qquad (2)$$

where $\langle \epsilon^2 \rangle$ is the mean squared displacement along one axis for a single step. For displacements that are uniformly distributed between $-\epsilon_0$ and $+\epsilon_0$, $\langle \epsilon^2 \rangle = \epsilon_0^2/3$. For $\Delta t = 25$ ns and $\epsilon_0 = 7.64482 \times 10^{-8}$ cm, eq 2 gives $D = 3.896 \times 10^{-8}$ cm^2/s, which is the translational diffusion coefficient for a 110 nm diameter sphere at 20 °C in water. Due to the small 25 ns time step, it was not considered necessary to draw the individual displacements from a Gaussian distribution. If two or more of the particles overlapped, then the configuration was rejected and a new one was created. Otherwise, the trial configuration was accepted for the simulation. If a particle reached the surface of the spherical sample volume, it was displaced by a distance $4\epsilon_0$ back toward the center of the sample volume. If that resulted in an excluded volume overlap with another particle, then the particle was placed at random at a point $R - 4\epsilon_0$ away from the center of the sample volume. Other than that of the excluded volume, there were no interactions between the particles.

For each time step of the simulation, the intensity was calculated using a Gaussian beam profile which is similar to that used by Aragon and Pecora[29]

$$P(\mathbf{r}) = \exp[-2(x^2 + y^2)/w_0^2] \exp[-2(z^2)/z_0^2] \qquad (3)$$

For each simulation, a count rate I_0 was chosen for a bead at the center of the container. Then for each time step, the intensity was calculated from

$$I'(t) = I_0 \sum_{i=1}^{N} P(\mathbf{r}_i) \qquad (4)$$

where $\mathbf{r}_i$ is the position of the ith bead at time step t and the sum goes over all of the N beads in the container. Poisson distributed noise was added to $I'(t)$ to obtain the simulated total intensity, $I(t)$, which can then be autocorrelated in the same manner as the experimental signal. I_0 was set to 1 MHz for a simulated laser intensity of 10 nW. This number was chosen to approximately match the experimentally observed peak count rates for the 110 nm diameter beads, when the count rate was averaged over intervals of 1 ms (1.35 MHz). For larger simulated laser intensities, I_0 was assumed to linearly scale with the power. The same values of w_0 and K that were determined from our experimental measurements were used both in the simulation and in fitting of the simulated correlation functions.

The manufacturer's specification for the APD claims a dead time of 50 ns, whose effect on the simulated fluorescence intensity was approximated by limiting the maximum number of counts that could be observed in any 25 ns time interval to 1 and by requiring that if a count was observed in the ith bin, then zero counts would be recorded for the $(i + 1)$th bin. This limits the simulated observed count rates to an absolute maximum of 20 MHz. Simulations were also performed in which neither of these restrictions were included, which corresponds to a detector with zero dead time. The autocorrelation function of the fluorescence intensity was calculated in a manner analogous to a hardware autocorrelator as described by Kojro et al.[30] For each simulated power, five simulations of 2.4×10^9 moves each were performed as described above. Each simulation represented 1 min of real time. The simulated correlation functions were then analyzed in the same manner as the measured autocorrelation functions to obtain five values of G_0, τ_D, and G_∞ for each intensity, which were then averaged.

For the simulations at the lowest simulated power, where the effects of dead time were negligible, the best-fit diffusion coefficient was $D = 3.9$ (± 0.2) $\times$ 10^{-8} cm^2/s, in good agreement with the theoretical value. Simulations with a range of particles for a detector with zero dead time also yielded best-fit diffusion coefficients in very good agreement with the expected results.

Simulations of Biased Diffusion at Various Potential Well Depths. The effect of an external potential on the measured FCS correlation function was studied in simulations with an external potential. The simulation procedure, which is a Brownian dynamics simulation,[31] was similar to that for the dead time simulations with the following changes. Instead of drawing random particle displacements from a uniform distribution for each time step, the displacement of a particle along a given coordinate axis is given by

$$\vec{r}(\Delta t) = \vec{r}(0) + \frac{D\vec{F}}{kT}\Delta t + \vec{R}(\Delta t) \qquad (5)$$

where D is the diffusion coefficient of the particle and Δt is the time for each move in the simulation, $\vec{r}(0)$ and $\vec{r}(\Delta t)$ are the positions of the particle before and after the move, $\vec{F}$ is the force due to the external potential acting on the particle at $\vec{r}(0)$, and $\vec{R}(\Delta t)$ is a vector of random deviates drawn from a Gaussian distribution with width

$$\sigma = \sqrt{2D\Delta t} \qquad (6)$$

Equations 5 and 6 are a much simplified version of eq 15 of Ermak and McCammon[31] and apply only for the case where hydrodynamic interactions between the spheres are ignored as they are in these simulations. For the biased diffusion simulations, $D = 1.54 \times 10^{-8}$ cm^2/s, the diffusion coefficient of a 290 nm diameter sphere, and $\Delta t = 200$ ns. The size of a physically meaningful time step is restricted to

$$\Delta t \gg \frac{mD}{kT} \qquad (7)$$

where m is the mass of the particle. Assuming the density of the polystyrene spheres is approximately the same as the density of water, for these simulations eq 7 becomes the condition $\Delta t \gg 5$ ns, which is satisfied here. As before, if the excluded volumes of two particles overlapped that configuration was rejected and a new one was generated. No other interaction between the particles was included in the simulation.

The simulated trapping force imparted onto a polystyrene particle was calculated for a 633 nm laser focused into water with an oil immersion lens. The force, F, is dominated by F_{grad}, the force due to the gradient of electric field[32]

$$F(r) = F_{grad}(r) = \left\{ \pi\epsilon_0 n_{water}^2 a^3 \left(\frac{(n_{particle}/n_{water})^2 - 1}{(n_{particle}/n_{water})^2 + 2} \right) \right\} \nabla |E(\vec{r})|^2 \quad (8)$$

where $E(\vec{r})$ is the electric field near the focus, a is the radius of the particle, $n_{particle}$ is the refractive index of particle, n_{water} is the refractive index of water, and ϵ_0 is the permittivity of a vacuum. Following Richards and Wolf, $E(\vec{r})$ equals the Debye integral of a highly focused linearly polarized Gaussian beam[33,34]

$$E(\vec{r}) = \frac{-ik}{2\pi} \int_\Omega \int P(\theta,\phi) \exp(ik(\vec{u}\cdot\vec{r})) \, d\Omega \qquad (9)$$

where $P(\theta,\phi)$ is the electric field right after the objective lens,

24436 *J. Phys. Chem. B, Vol. 110, No. 48, 2006*

Kuyper et al.

$\vec{u}$ is the unit vector in the direction of propagation of the light, and $k = 2\pi/\lambda$. Radiation pressure caused by the scattering or absorption of light by the particle is negligible compared to F_{grad}, due to the low laser power and the small particle size.[35] In this calculation, the light is propagating along the z axis and is polarized along the x direction. The polarization of the light breaks the symmetry between the x and y axes, and thus the resulting forces along the x and y axes, while similar, are not identical. Equations 6 and 7 are used to provide a force field that approximates the one experienced by a particle in the FCS experiment. As will be discussed below, the simulation uses only the relative magnitudes and directions of the calculated force field, and the value of any constants that are independent of position are not relevant.

Equations 8 and 9 were used to calculate a force field for a cubic lattice of points with a spacing of $(0.04)\lambda$, where $\lambda = 633$ nm is the wavelength of the trapping laser. The force field was calculated for points extending from -2λ to $+2\lambda$ in the x and y directions and from -4λ to $+4\lambda$ in the z direction; the origin of the system was placed at the focal point of the trapping laser beam. For those points between the cubic lattice of points, the force was obtained by linear interpolation of the force vectors of the eight lattice points that surround it. The force on any particle outside the cubic lattice was set to zero. The spacing of the points in the lattice limits the spatial resolution of our force field to approximately $(0.02)\lambda \approx 13$ nm, which was judged to be sufficient for these simulations.

The force field was scaled by a multiplicative factor to produce a desired well depth, U, so only the direction and relative magnitude of the force from the above calculation were needed for the biased diffusion simulations. The reversible work necessary to remove a particle from the force field by moving it along one of the coordinate axes is

$$W = -\int_0^L F_s(s)\, \mathrm{d}s \qquad (10)$$

where s is x, y, or z, $F_s(s)$ is the s component of the force for points on the s axis, and L is a positive constant large enough such that $F_s(s) = 0$ for both $s > L$ and $s < -L$. The well depth, W, for the calculated force field was taken to be the average of the six reversible works calculated by integrating eq 10 along each of the three axes in both the positive and negative directions. The six numerical results agreed to within ±0.25%. The forces were then scaled by (U/W), where U is the desired value of the potential well depth for a given simulation. For $U = 1k_BT$, the resulting forces are shown in Figure 1A and the potential energy is shown in Figure 1B. The corresponding plots for any other value of the well depth can be obtained by multiplying the numbers on the ordinate in parts A and B of Figure 1 by the desired value of U expressed in units of k_BT.

The intensities for each configuration of beads were calculated using eqs 3 and 4, and the results were autocorrelated and fit as before. Simulations were performed for three different values of the well depth ($U = 0$, 1, and $3k_BT$, where k_B is Boltzmann's constant and T is the temperature). For each value of U, simulations were run with $N = 10$ particles in the sample volume. Each simulation consisted of 1.2×10^9 moves and represented 4 min of real time. Ten simulations were performed for each value of U. The temperature for these simulations was set at 21.5 °C, which was judged to be close to the average room temperature of the laboratory where the FCS measurements were made. The viscosity of water was 0.966 cP. As before, $G(\tau)$ was calculated and fit for each simulation in the same manner as that for the experimental data.
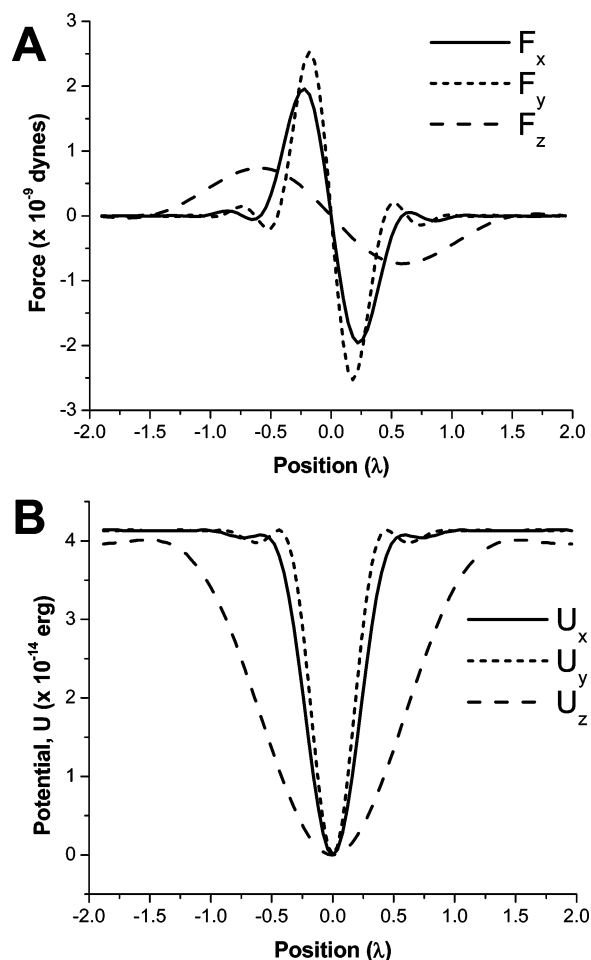

Figure 1. (A) Simulated forces due to trapping for points on the three coordinate axes. The forces were scaled to yield a potential energy well depth of $1k_BT$. Solid line, F_x at points along x axis; dashed line, F_y at points along y axis; long dashed line, F_z at points along z axis. (B) Potential energies due to trapping for points on the three coordinate axes. The forces were scaled to yield a potential energy well depth of $U = 1k_BT$. The plot for any other well depth can be obtained by simply multiplying the numbers on the ordinate by the desired well depth in units of k_BT. Solid line, potential energy at points along x axis; dashed line, potential energy at points along y axis; long dashed line, potential energy at points along z axis. The potential along the z axis reaches $1k_BT$ near ±4λ. The positions are given in units of $\lambda = 633$ nm, the wavelength of the trapping laser.

The simulations with $U = 0$ provide a check on the simulation protocol and program. Fits of the correlation function for the case $U = 0$ yielded a best-fit value for the diffusion coefficient of $D = 1.52 \, (\pm0.01) \times 10^{-8}$ cm^2/sec, in good agreement with the theoretical value. As an additional check, simulations were also run using a single 2 nm diameter particle with $U = 25k_BT$. For these simulations, the particle was started at the bottom of the potential well and the well depth was large enough that the particle did not escape during the simulation. The choice of a smaller particle size in this instance was simply to speed up the equilibration of the simulation by giving the particle a larger diffusion coefficient, and so from eq 6, the simulation would use larger step sizes. So long as the particle spends most of its time near the bottom of the potential well, the equilibrium distribution should be approximately Gaussian with width

$$\sigma_s = \sqrt{\frac{k_BT}{k_s}} \qquad (11)$$

where k_s is the force constant along the s axis near the origin

Accurate Sizing of Nanoparticles

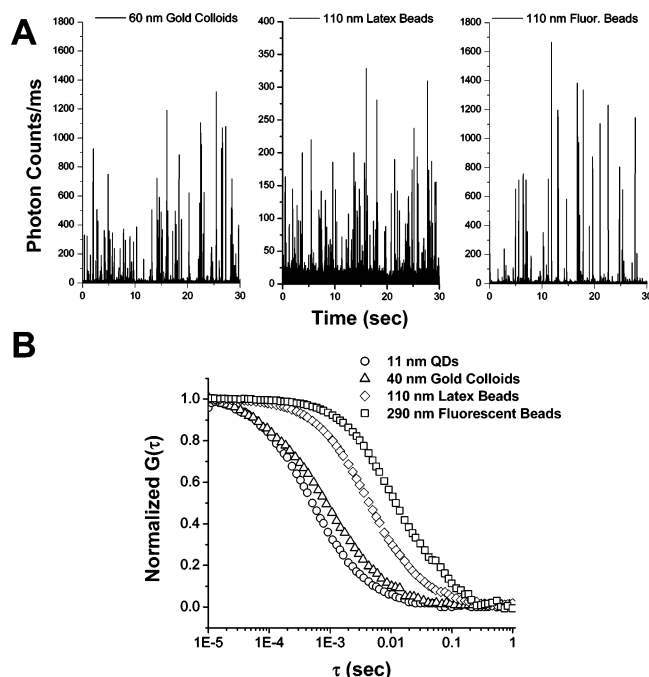*J. Phys. Chem. B, Vol. 110, No. 48, 2006* **24437**

Figure 2. (A) Backscattering intensity traces for gold colloids (diameter = 60 nm, left panel), nonfluorescent latex beads (diameter = 110 nm, center panel), and fluorescent latex beads (diameter = 110 nm, right panel). The time resolution was 1 ms, and each photon burst corresponded to a particle entering and exiting the probe volume. (B) Autocorrelation of burst events provided the diffusion coefficients for particles with diameters ranging from 11 nm for quantum dots, 40 nm for gold colloids, 110 nm for nonfluorescent latex beads, to 290 nm for fluorescent beads.

and eq 11 is just the expected result for a particle trapped in a harmonic potential. The *x, y,* and *z* force constants for our force field equal the negative of the slope of the force versus position curves in Figure 1A near the origin. After scaling to obtain a well depth of 25 k_BT, the force constants are $k_x = 4.93 \times 10^{-3}$, $k_y = 7.53 \times 10^{-3}$, and $k_z = 7.16 \times 10^{-4}$ dyn/cm. Using eq 11 we get $\sigma_x = 2.86 \times 10^{-6}$, $\sigma_y = 2.32 \times 10^{-6}$, and $\sigma_z = 7.52 \times 10^{-6}$ cm. The largest of these widths, σ_z, corresponds to a distance of 0.12λ, which as can be seen from Figure 1B indicates that the particle spends most of its time near the bottom of the potential well. These predicted results can be compared with the results of the five single-particle simulations of 1.2×10^9 moves each, where the position of the particle was recorded every 5 000 moves to produce an equilibrium distribution of particle positions within the potential well. These distributions were fit to a Gaussian, to yield best-fit widths (σ_s^{bf}) of $\sigma_x^{bf} = 2.85 \ (\pm 0.28) \times 10^{-6}$, $\sigma_y^{bf} = 2.13 \ (\pm 0.25) \times 10^{-6}$, and $\sigma_z^{bf} = 7.28 \ (\pm 0.45) \times 10^{-6}$ cm, in good agreement with the values above.

Results and Discussion

Sizing Nanoparticles with Confocal Correlation Spectroscopy. While confocal correlation spectroscopy can size particles in batch volumes such as dynamic light scattering, a unique advantage lies in its ability to size both nonfluorescent and fluorescent particles in real time and in small-volume (pL– nL) samples. Accurate sizing of nanoparticles with ranging compositions and diameters depended on several factors, such as particle composition, signal intensity, background level, and laser power. Figure 2A shows burst intensities at 10 nW (488 nm) for slightly different concentrations of 60 nm diameter gold colloids, 110 nm nonfluorescent latex beads, and 110 nm

fluorescent beads. In the backscattering mode, we observed strong scattering from the 60 nm gold colloids, which peaked at ~1 300 counts/ms. In comparison, 110 nm latex beads peaked at ~350 backscattered photon/ms, a reflection that polystyrene beads are weaker scatterers than gold particles. Because the backscattering mode was recorded without a band-pass filter, excess Rayleigh background scattering from solution limited the sensitivity of the backscattering mode in comparison with the fluorescence mode, which had low backgrounds from Raman scattering from water and was capable of detecting single dye molecules. Also, backscattering off the glass coverslip plagued sampling when the laser focus was placed closer than ~5 μm from the substrate. As a result, for each run, the probe volume was positioned ~25 μm above the glass surface. In the fluorescence mode, QDs of ~11 nm in diameter composing both the core and shell were readily measured. In both the backscattering and fluorescence modes, reproducibility and error were primarily caused by the quality of the sample as aggregates caused unwanted inaccuracies in the measurements. In addition, more concentrated solutions allowed for faster acquisition and more accurate measurements due to the larger number of passes that were averaged over the duration of the experiment.

With proper care in acquiring measurements, confocal correlation spectroscopy was versatile for sizing a wide range of nanoparticles (see Figure 2B). The method can accurately size particles composed of gold and polystyrene, as well as CdSe QDs and dye-doped fluorescent polystyrene nanospheres.

Dependence of Measured Particle Size on Laser Power. For many particles, measurements with low excitation powers sufficed to provide an accurate size; however, for smaller, less bright particles, low powers can pose a problem due to poor signal-to-noise ratios. Unfortunately, measured particle sizes appeared to be power dependent and were inaccurate at higher powers. First suggested by Chiu and Zare, this power dependence has been coined biased diffusion and is believed to be due to optical trapping forces imparted onto particles as they enter into the laser beam. These forces slow the trajectory of the particle through the beam and also cause a deviation in the probability that a particle will enter the beam.[21] These effects have been characterized for single dye molecules; Klenerman and co-workers reported that the measured diffusion time of individual rhodamine 6G molecules increased linearly with power ranging from 300 to 900 μW and that the probability of observing a particle deviated from Poisson statistics.[22] In addition, Chirico and co-workers reported a similar linear increase in diffusion time as a function of power but found that two-photon microscopy does not render a power dependence and could be used to overcome such artifacts.[23] Several possibilities have been suggested to explain the effect of power on particle diffusion. Most notably, the gradient force induced by an optical trap can disrupt the path of a freely diffusing particle enough to slow its movement across the probe volume. At constant powers, the magnitude of this interaction primarily depends upon the polarizability of the particle,[20] which is dependent upon particle volume, composition, and for fluorescent particles the number of dye molecules doped inside. In addition, the deviation has also been attributed to resonant versus nonresonant forces, which for single rhodamine 6G molecules biased diffusion is claimed to be enhanced due to excitation with a laser on resonance with the dye absorption.[22] Last, another potential artifact results from molecular saturation of the molecules as they transit the probe volume and can indirectly affect the probe volume measurements used to determine the diffusion time.[36–38]
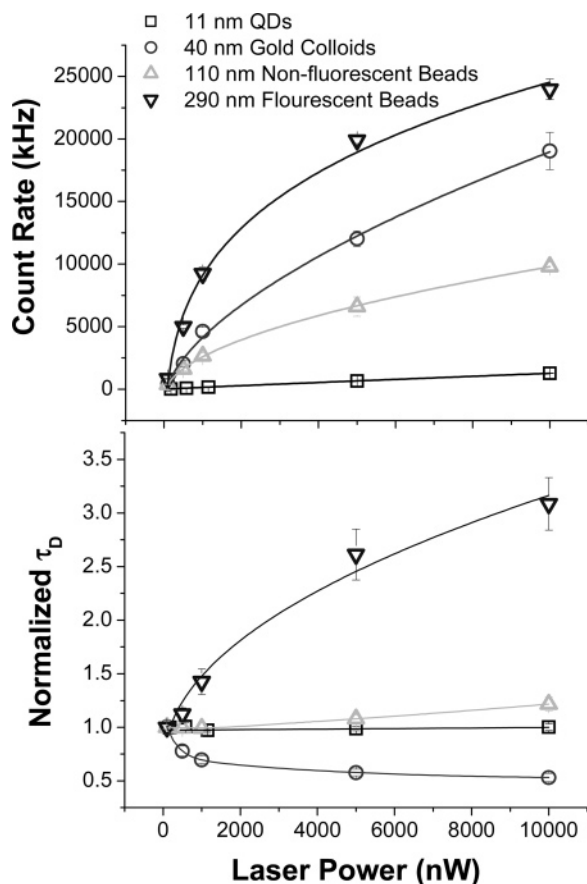
Figure 3. (Upper panel) Count rates increased nonlinearly with laser power and varied for each type of particle as noted here: 11 nm diameter QDs (squares), 60 nm diameter gold colloids (circles), 110 nm diameter nonfluorescent latex beads (triangles), and 290 nm diameter fluorescent beads (upside-down triangles). (Lower panel) Normalized diffusion times (τ_D) for each type of particle followed different trends and exhibited different magnitudes of deviation.

In contrast to previous reports on single molecules, for larger nanoscale particles, we found that the power dependence of the diffusion times was nonlinear and different for each particle type and diameter. As shown in Figure 3, QD intensity increased linearly with power, but we observed no deviation in the measured particle with laser power (from a minimum power of 250 nW needed for detection out to 10 μW). In contrast, the 110 nm nonfluorescent latex beads—even more so the 290 nm fluorescent beads—showed problematic deviations from their true size as power was increased from 10 nW to 10 μW. For fluorescent particles, brighter beads had a greater deviation of the diffusion time from their true values as measured at low powers. Moreover, intensity was related to volume as well as the number of dyes in the particle. Interestingly, the gold colloids showed an opposite effect with increasing power: the diffusion times decreased rather than increased. We are currently working to understand the result for the gold colloids; however, this effect may be attributed to possible heating of the nanoparticle due to absorption or to a scattering force that pushes the colloids out of the probe volume more quickly as power is increased. Nevertheless, for accurate sizing, low laser powers can be used where the diffusion times of gold colloids do not show deviations.

Detector Dead Time Causes a Deviation in the Apparent Size and Local Concentration of Particles. A possible source of the power dependence of the apparent size and local concentration of particles is the dead time of the detector. The detector dead time, which is the time after the detection of a
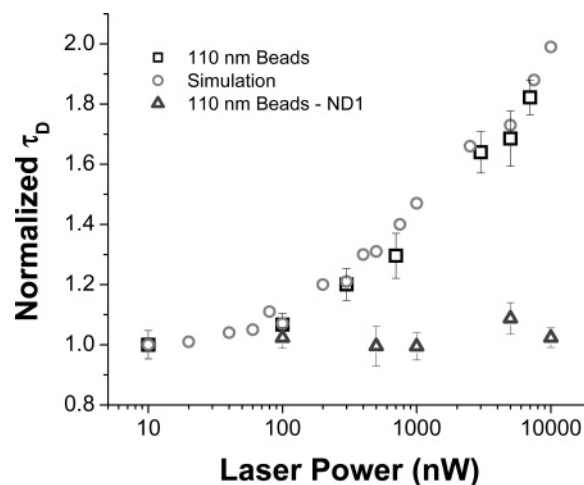

Figure 4. Normalized diffusion times of 110 nm diameter beads without intensity attenuation (boxes) and with attenuation by a neutral density filter (ND 1.0) placed in front of the detector (triangles). Simulations that factored in dead time of the detector fit well with the raw, unattenuated data (circles).

photon during which the detector is blind to the arrival of additional photons, has long been known to affect the observed distribution of photon counts,[17,25,26] and expressions for the effect of the detector dead time on the FCS correlation function have been derived to first order as a ratio of the detector dead time to the sampling interval.[17,26] Furthermore, these effects have also been investigated for FCS measurements on single dye molecules.[39]

The presence of a finite dead time in the detector or electronics will cause the loss of some photons. While the average count rate (Figure 3) seems modest enough given the dead time of our detector ($\sim$50 ns), when the fluorescent particle is near the center of the probe volume, the count rate, averaged over 1 ms, can be as high as 1.35 MHz with a 10 nW of excitation power. Even at the lowest power used (10 nW), the number of photons counted is reduced by approximately 7% due to the detector dead time. As the power is increased, the fraction of photons lost can become quite large. In addition, peak shapes for each burst event will increasingly deviate from those defined by the fixed excitation profile of the probe volume. Notably, the maximum intensity flattens in relation to the width of the burst, thereby resulting in the appearance that diffusion time increases as a function of power. Figure 4 shows three curves of normalized diffusion times (τ_D) for 110 nm diameter fluorescent beads freely diffusing and measured at varied laser powers. The uncorrected diffusion time (squares) increased nonlinearly with power and fit well to simulations of 110 nm beads (circles) diffusing in to and out of a probe volume of the same dimensions and with a simulated detector dead time of 50 ns. In practice, placement of a neutral density filter in front of the detector resulted in peak intensities that did not register over $\sim$1.5 MHz, thus causing no deviation within error for the measured particle size out to 10 μW (triangles).

Another effect that has been attributed to biased diffusion is the increase in local particle concentration around the beam focus. For brighter particles, we also found the number of particles per unit volume, or the reciprocal of the y-intercept in the autocorrelation curve, increased nonlinearly with power. Figure 5A shows the effective increase in the frequency and duration of photon bursts over a given period of time. At low power (10 nW), we only saw $\sim$30 burst events over 60 s. In contrast, at high power (100 μW) we recorded $\sim$65 burst events and the bursts were significantly longer in duration. Similar to

Accurate Sizing of Nanoparticles

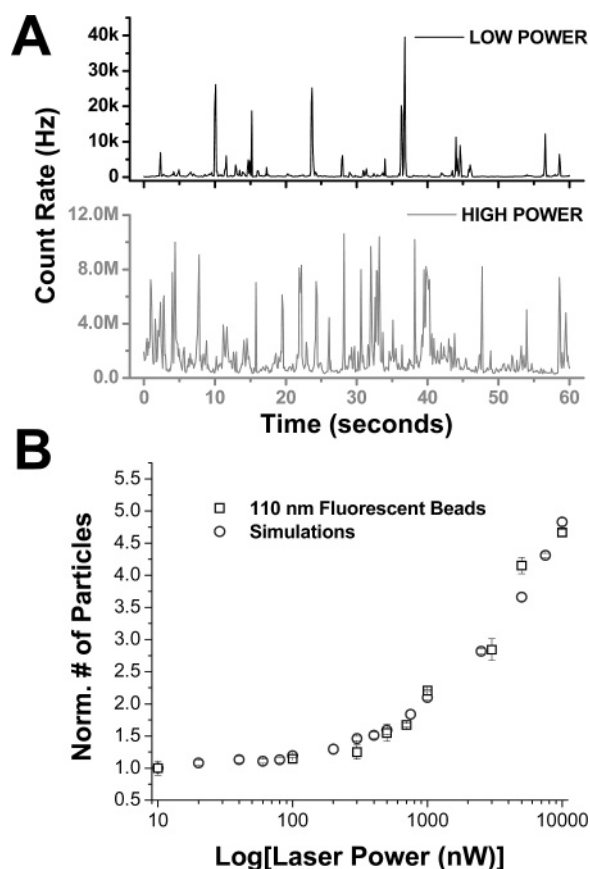*J. Phys. Chem. B, Vol. 110, No. 48, 2006* **24439**

Figure 5. (A) Photon-burst traces from fluorescent beads (diameter = 110 nm) diffusing in and out of the probe volume. At low powers (10 nW), the burst frequency represented true local concentration of nanoparticles; at high powers (100 μW), the local concentration of particles appeared to increase as evinced by more frequent bursts. (B) Normalized number of particles present in the probe volume obtained from experiments (circles) and simulation (squares) fit well.

the deviation in diffusion time, dead-time artifacts from the detector also caused an apparent increase in concentration or the average number of particles contained within the probe volume. As shown in Figure 5B, the normalized number of particles per unit volume was calculated from the intercept of the correlation curve from experiments and compared with simulations that factored in the dead-time of the detector. For both diffusion times and particle concentration, without proper care and awareness this effect can be incorrectly interpreted as a biasing of diffusion of particles in solution.

Palmer and Thompson derived an expression for the FCS correlation function to first order in τ_{dt}/T, where τ_{dt} is the dead time of the detection system and T is the sampling interval.[26] Some of these correction terms to $F(t)$ (the correlation function in the absence of the detector dead time) are proportional to τ_{dt}/T and have the same time dependence as $F(t)$. As a result, their inclusion will not affect the determination of the D, though they might affect the determination of $G(0)$. However, other terms are proportional to $\tau_{dt}q/T$, where q is the average number of photons per time interval, and have a different time dependence from $F(t)$. For large count rates, $\tau_{dt}q$ can be comparable to T and so these terms can affect the determination of both D and $G(0)$, and our results here are in agreement with their results. However, for smaller count rates, such as for our measurements taken with 10 nW excitation power, the effect of these additional terms is expected to be negligible, as was demonstrated by our simulations that showed best-fit diffusion
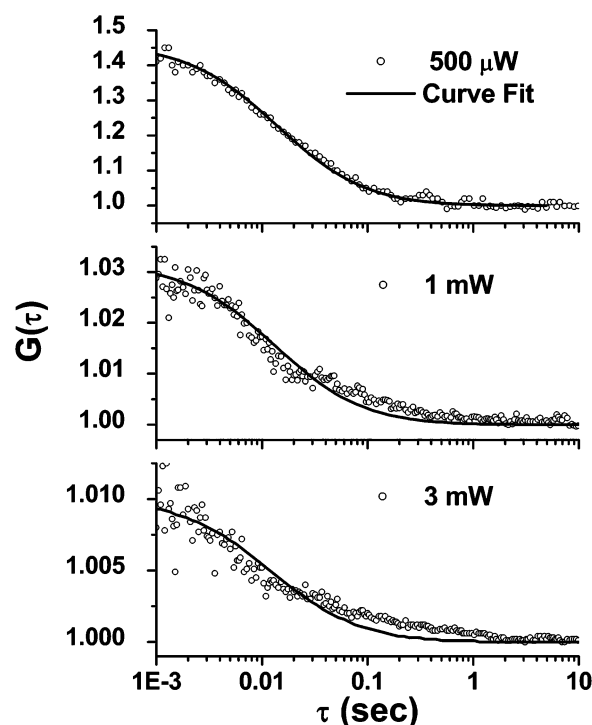

Figure 6. CCS curves recorded for fluorescent beads (diameter = 290 nm) under the resonant condition as 488 nm laser light was increased from 500 μW to 3 mW. As the power was increased, theoretical curves (solid black lines) produced by the 3D FCS equation no longer fit the data.

coefficients in good agreement with the theoretical diffusion coefficients for the lowest excitation power.

Resonant and Nonresonant Conditions for Biased Diffusion. At lower powers (10 nW–10 μW), the increases in diffusion times measured with confocal correlation spectroscopy were a result of detector dead-time artifacts. However, at higher powers (>1 mW), we observed that biased diffusion does appear to occur and can be detected under both resonant and nonresonant conditions. Theoretical predictions have suggested that trapping enhancements can be achieved when using a beam that is resonant with the absorption maximum of the particles being analyzed.[40] Furthermore, this resonance enhancement has been suggested as a potential way to sort selectively particles based upon the resonance wavelength.[41] Yet, we found that trapping enhancement for resonant versus nonresonant forces was only slightly different for heavily dye-doped, fluorescent beads absorbing at 488 nm. For resonant conditions (Figure 6), we increased laser power at 488 nm from 10 nW to 3 mW and added neutral density filters to ensure that signal from fluorescent, 290 nm diameter beads did not peak above 1.5 MHz. For nonresonant conditions (Figure 7A), the focus of the 488 nm beam and the focus of a 632.8 nm HeNe beam were positioned in the same location. In this case, the 488 nm beam was held constant at 10 nW of power to excite fluorescence from freely diffusing beads. Power of the HeNe beam was increased incrementally from 10 nW to 3 mW. Within error, no change in the diffusion times of the beads was recognizable until ~1 mW for both conditions. As shown in Figure 7A, the relative contribution of longer correlation times increased while shorter times decreased. We believe that the increase in longer diffusion times can be attributed to passes where the bead entered fully into the probe volume and was partially trapped along its trajectory. Because of these changes in the autocorrelation function, the 3D FCS equation used to calculate the diffusion time no longer fit the data. Interestingly, both the resonant and
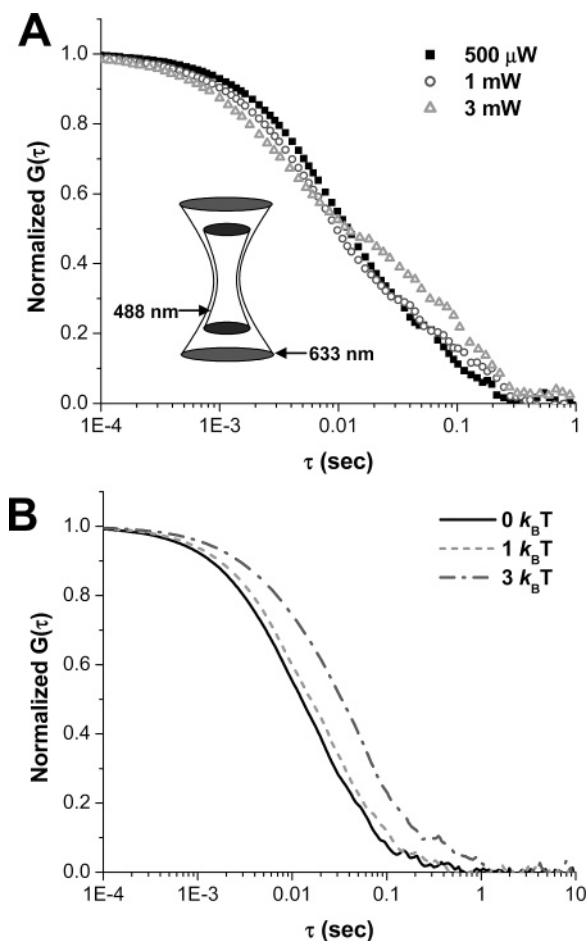
24440 *J. Phys. Chem. B, Vol. 110, No. 48, 2006*

Kuyper et al.

Figure 7. (A) CCS curves recorded for fluorescent beads (diameter = 290 nm) under the nonresonant condition where the focus of the 633 nm laser beam was positioned in-line with the focus of the 488 nm laser beam. Fluorescence bursts were recorded using 10 nW of 488 nm light, but the power of the 633 nm beam was increased from 500 μW to 1 mW and then to 3 mW. (B) Simulated correlation curves were calculated for particles (diameter = 290 nm) that interacted with potential wells with depths of $0k_BT$ (solid line), $1k_BT$ (dashed line), and $3k_BT$ (dash-dot line).

nonresonant condition showed a deviation in correlation times at similar powers; however, for the resonant condition longer time correlations appear to span past 1 s. Unfortunately, we observed saturation of fluorescence from the beads at ~100 μW, at which point background from the laser and sample decreased the signal-to-background ratio (SBR) for burst events from the 290 nm beads. As a result, the correlation curves taken in the milliwatt range were noisy in comparison to ones obtained at lower powers, such as the 500 μW data shown in Figure 6A. Nevertheless, the observations suggest that biased diffusion does occur at high powers for both conditions.

In addition to experimental observations, we simulated the non-resonant-condition experiments (Figure 7B) to define the range of potential well depths, which were expressed in relation to k_BT, experienced by the beads as they traversed the probe volume. The simulations suggest that the interaction of the laser with the beads is not noticeable until >$1k_BT$. At $3k_BT$, the deviation observed in the simulation was similar in magnitude to the experimentally measured deviation shown for 3 mW. However, the experimental correlation function is bimodal in the presence of the trapping laser. One component exhibits a smaller decay time than the single decay time for the correlation function in the absence of the trapping laser and one exhibits a larger decay time. These combine to produce the pronounced

bulge in the correlation function in Figure 7A. In contrast, the simulated correlation functions exhibit only the larger decay time. We believe that these differences were caused by a small misalignment between the red and blue focal spots. Experimentally, the perfect alignment of these two diffraction-limited focal volumes is challenging.

Conclusions

This paper characterizes confocal correlation spectroscopy for the accurate sizing of nanoparticles. At low laser powers (10 nW–10 μW), we found that high-frequency (>1.5 MHz) burst events from nanoparticles showed detector dead-time artifacts, which resulted in the appearance of a nonlinear increase in diffusion times (or particle size) and particle concentrations with laser power. At higher powers (>1 mW), resonant and nonresonant trapping forces caused an increasing contribution of longer particle transit times. Here, the change in the shape of the autocorrelation curve provides a convenient way to assess whether biased diffusion is occurring. With the increasing interest in both nanotechnology and small-volume analysis and control, we believe that proper use of confocal correlation spectroscopy will offer a useful way to accurately measure the sizes of nanoscale particles and macromolecular complexes.

References and Notes

(1) Hashida, M.; Kawakami, S.; Yamashita, F. *Chem. Pharm. Bull.* **2005**, *53*, 871.
(2) Medina, O. P.; Zhu, Y.; Kairemo, K. *Curr. Pharm. Des.* **2004**, *10*, 2981.
(3) Harris, K. M.; Sultan, P. *Neuropharmacology* **1995**, *34*, 1387.
(4) Portney, N. G.; Ozkan, M. *Anal. Bioanal. Chem.* **2006**, *384*, 620.
(5) Santra, S.; Dutta, D.; Walter, G. A.; Moudgil, B. M. *Technol. Cancer Res. Treat.* **2005**, *4*, 593.
(6) Wiesendanger, R. *Scanning Probe Microscopy and Spectroscopy: Methods and Applications*; Cambridge University Press: New York, 1994.
(7) Cohen, S. H.; Lightbody, M. L. *Atomic Force Microscopy/Scanning Tunneling Microscopy 3*; Kluwer Academic/Plenum Publishers: New York, 1999.
(8) Berne, B. J.; Pecora, R. *Dynamic Light Scattering: With Applications to Chemistry, Biology, and Physics*; Wiley: New York, 2000.
(9) Chan, E. M.; Mathies, R. A.; Alivisatos, A. P. *Nano Lett.* **2003**, *3*, 199.
(10) Jahn, A.; Vreeland, W. N.; Gaitan, M.; Locascio, L. E. *J. Am. Chem. Soc.* **2004**, *126*, 2674.
(11) Khan, S. A.; Gunther, A.; Schmidt, M. A.; Jensen, K. F. *Langmuir* **2004**, *20*, 8604.
(12) Krishnadasan, S.; Tovilla, J.; Vilar, R.; deMello, A. J.; deMello, J. C. *J. Mater. Chem.* **2004**, *14*, 2655.
(13) Lewis, P. C.; Graham, R. R.; Nie, Z.; Xu, S.; Seo, M.; Kumacheva, E. *Macromolecules* **2005**, *38*, 4536.
(14) He, M.; Edgar, J. S.; Jeffries, G. D. M.; Lorenz, R. M.; Shelby, J. P.; Chiu, D. T. *Anal. Chem.* **2005**, *77*, 1539.
(15) Tan, Y.-C.; Hettiarachchi, K.; Siu, M.; Pan, Y.-R.; Lee, A. P. *J. Am. Chem. Soc.* **2006**, *128*, 5656.
(16) Magde, D.; Elson, E. L.; Webb, W. W. *Phys. Rev. Lett.* **1972**, *29*, 705.
(17) Koppel, D. E. *Phys. Rev. A: At., Mol., Opt., Phys.* **1974**, *10*, 1938.
(18) Saffarian, S.; Elson, E. L. *Biophys. J.* **2003**, *84*, 2030.
(19) Wohland, T.; Rigler, R.; Vogel, H. *Biophys. J.* **2001**, *80*, 2987.
(20) Ashkin, A.; Dziedzic, J. M.; Bjorkholm, J. E.; Chu, S. *Opt. Lett.* **1986**, *11*, 288.
(21) Chiu, D. T.; Zare, R. N. *J. Am. Chem. Soc.* **1996**, *118*, 6512.
(22) Osborne, M. A.; Balasubramanian, S.; Furey, W. S.; Klenerman, D. *J. Phys. Chem. B* **1998**, *102*, 3160.
(23) Chirico, G.; Fumagalli, C.; Baldini, G. *J. Phys. Chem. B* **2002**, *106*, 2508.
(24) Kuyper, C. L.; Budzinski, K. L.; Lorenz, R. M.; Chiu, D. T. *J. Am. Chem. Soc.* **2006**, *128*, 730.

Accurate Sizing of Nanoparticles

J. Phys. Chem. B, Vol. 110, No. 48, 2006 **24441**

(25) Johnson, F. A.; Jones, R.; McLean, T. P.; Pike, E. R. *Phys. Rev. Lett.* **1966**, *16*, 589.

(26) Palmer, A. G.; Thompson, N. L. *Rev. Sci. Instrum.* **1989**, *60*, 624.

(27) Hamilton, K. G.; James, F. *Comput. Phys. Commun.* **1997**, *101*, 241.

(28) Gebe, J. A.; Delrow, J. J.; Heath, P. J.; Fujimoto, B. S.; Stewart, D. W.; Schurr, J. M. *J. Mol. Biol.* **1996**, *262*, 105.

(29) Aragon, S. R.; Pecora, R. *J. Chem. Phys.* **1976**, *64*, 1791.

(30) Kojro, Z.; Riede, A.; Schubert, M.; Grill, W. *Rev. Sci. Instrum.* **1999**, *70*, 4487.

(31) Ermak, D. L.; McCammon, J. A. *J. Chem. Phys.* **1978**, *69*, 1352.

(32) Harada, Y.; Asakura, T. *Opt. Commun.* **1996**, *124*, 529.

(33) Richards, B.; Wolf, E. *Proc. R. Soc. London, Ser. A* **1959**, *253*, 358.

(34) Boivin, A.; Wolf, E. *Phys. Rev. B: Solid State* **1965**, *138*, 1561.

(35) Tlusty, T.; Meller, A.; Bar-Ziv, R. *Phys. Rev. Lett.* **1998**, *81*, 1738.

(36) Berland, K. M.; Shen, G. *Appl. Opt.* **2003**, *42*, 5566.

(37) Marrocco, M. *Appl. Opt.* **2004**, *43*, 5251.

(38) Nagy, A.; Wu, J.; Berland, K. M. *J. Biomed. Opt.* **2005**, *10*, 044015.

(39) Nishimura, G.; Kinjo, M. *Appl. Opt.* **2005**, *44*, 3458.

(40) Iida, T.; Ishihara, H. *Phys. Rev. Lett.* **2003**, *90*, 057403.

(41) Li, H.; Zhou, D.; Browne, H.; Klenerman, D. *J. Am. Chem. Soc.* **2006**, *128*, 5711.